Myosin Id localizes in dendritic spines through the tail homology 1 domain

1   **Title**

2   Myosin Id localizes in dendritic spines through the tail homology 1 domain

3

4   **Authors**

5   Ryusuke Koshida*, Saki Tome, Yosuke Takei*

6

7   **Affiliations**

8   Department of Anatomy and Neuroscience, Faculty of Medicine, University of Tsukuba, Tsukuba

9   305-8577, Japan

10

11   ***Corresponding authors**

12   Email addresses: rkoshida@md.tsukuba.ac.jp (R. Koshida), ytakei@md.tsukuba.ac.jp (Y. Takei)

13

Abstract

Dendritic spines, the postsynaptic compartments at excitatory synapses, are capable of changing their shape and size to modulate synaptic transmission. The actin cytoskeleton and a variety of actin-binding proteins play a critical role in the dynamics of dendritic spines. Class I myosins are monomeric motor proteins that move along actin filaments using the energy of ATP hydrolysis. Of these class I myosins, myosin Id, the mammalian homolog of *Drosophila Myo31DF*, has been reported to be expressed in neurons, whereas its subcellular localization in neurons remained unknown. Here, we investigated the subcellular localization of myosin Id and determined the domain responsible for it. We found that myosin Id is enriched in the F-actin-rich pseudopodia of HEK293T cells and in the dendritic spines of primary hippocampal neurons. Both deletion and substitution of the tail homology 1 (TH1) domain drastically diminishes its colocalization with F-actin. In addition, the mutant form lacking the TH1 domain is less distributed in dendritic spines than is the full-length form. Taken together, our findings reveal that myosin Id localizes in dendritic spines through the TH1 domain.

Introduction

Dendritic spines are postsynaptic compartments that receive excitatory neurotransmitters, such as glutamate, released from the presynaptic terminals. The changing in the shape and size of dendritic spines in response to environmental stimuli is an essential process for synaptic plasticity (Caroni et al., 2012). The actin cytoskeleton is a major component of dendritic spines and plays a critical role in their structural dynamics (Cingolani and Goda, 2008; Hotulainen and Hoogenraad, 2010). In addition, a variety of actin-binding proteins such as Arp2/3 (Spence et al., 2016), ADF/cofilin (Gu et al., 2010), and myosins (Rex et al., 2010; Ryu et al., 2006) are involved in regulation of dendritic spine morphology. The importance of understanding the regulatory mechanisms underlying the dynamics of dendritic spines has been increasingly emphasized because abnormal spine morphology is associated with neurodevelopmental disorders such as autism spectrum disorder (ASD) and schizophrenia (Dölen et al., 2007; Penzes et al., 2011).

Myosins are motor proteins that move along actin filaments by using the energy of ATP hydrolysis (Kneussel and Wagner, 2013). Myosins form a large family that consists of approximately 40 members. Of these, class I myosins (myosin Ia –Ih) are monomeric proteins that carry three different domains in common, namely an N-terminal motor domain, a neck domain, and a C-terminal tail homology 1 (TH1) domain (McConnell and Tyska, 2010; McIntosh and Ostap, 2016). The motor

3

49 domain contains ATPase and an actin-binding site. The TH1 domain is capable of binding to anionic

50 phospholipids. The neck domain resides between the former two domains and contains IQ motifs

51 that bind to calmodulin. Subcellular localization of myosin I isoforms has been assumed to be

52 determined by its affinity to actin or phospholipids. In fact, class I myosins act as a linker between

53 actin filaments and the plasma membrane in a variety of cell types (Bose et al., 2004; Komaba and

54 Coluccio, 2010; Patino-Lopez et al., 2010; Tyska and Mooseker, 2002).

55 　　The tendency of class I myosins to localize actin-rich protrusions prompted us to hypothesize that

56 they are enriched in actin-rich dendritic spines. In particular, myosin Id is a promising candidate

57 because it is expressed in neurons (Benesh et al., 2012). In addition, a linkage analysis suggesting

58 that myosin Id is a potential risk gene for ASD (Stone et al., 2007) implied that myosin Id might play

59 an important role in dendritic spines. Myosin Id is a homolog of *Drosophila* myosin IA (encoded by

60 *Myo31DF*), which is essential for the left-right visceral asymmetry of *Drosophila* organs (Hozumi et

61 al., 2006). In mammals, myosin Id is highly enriched in the microvilli of intestinal epithelial cells

62 (Benesh et al., 2010). However, its subcellular localization in neurons remained unknown.

63 　　Here, we showed that myosin Id localizes in the dendritic spines of primary hippocampal neurons.

64 We also found that the TH1 domain is critical for its distribution in dendritic spines.

65

66   **Materials and Methods**

67   *Mice*

68   All experiments using CD1 and C57BL/6J mice were carried out according to the Guide for the

69   Care and Use of Laboratory Animals at the University of Tsukuba.

70

71   *DNA constructs*

72   The open reading frame of the myosin Id gene was amplified from mouse brain cDNA using PCR

73   and subcloned into a pEGFP-C1 vector (Clontech) so that EGFP was fused to its N-terminus. Mutant

74   vectors lacking the conserved sequence corresponding to the actin-binding site of *Drosophila*

75   homolog myosin IA (Δ584–594) (Morgan et al., 1994), the TH1 domain (ΔTH1), or the motor

76   domain (IQ + TH1) and mutant vectors in which each of the "signature basic residues" in the TH1

77   domain is substituted with alanine (K865A, R875A) (Hokanson and Ostap, 2006) were prepared

78   using a PrimeSTAR Mutagenesis Basal Kit (TaKaRa).

79

80   *Cell cultures and transfection*

81   Primary hippocampal neurons were prepared from mouse embryos at embryonic day 16.5. Briefly,

82   the hippocampi were dissected and digested with 0.25% trypsin/HBSS for 15 minutes at 37 °C. The

83 cells were dissociated by gentle pipetting and plated at a density of 8×10^4 cells on 12-well plates. In

84 advance, coverslips were placed on the well and coated with 0.04% polyethylenimine and 1 mg/ml

85 poly-L-lysine. Primary hippocampal neurons were maintained in MEM supplemented with 6 g/l

86 glucose, 1 mM sodium pyruvate, 2 mM GlutaMax (Gibco), and 2% NeuroBrew-21 (Miltenyi Biotec).

87 HEK293T cells were cultured in DMEM supplemented with 10% heat-inactivated fetal bovine serum

88 and 1% Pen Strep (Gibco). Both groups of cells were transfected with vectors using Lipofectamine

89 2000 (Invitrogen).

90

91 *Quantitative RT-PCR*

92   Total RNA was extracted from mouse brains and primary hippocampal neurons using NucleoSpin

93 RNA (Macherey-Nagel) and cDNA was synthesized using a High-Capacity RNA-to-cDNA Kit

94 (Applied Biosystems) according to the manufacturer's instructions. Real-time PCR was performed

95 on an Eco Real-time PCR System (Illumina) with THUNDERBIRD SYBR qPCR Mix (Toyobo).

96 The analyses were performed in duplicate. Relative expression levels were calculated with the $2^{-\Delta\Delta Ct}$

97 method using HPRT as an internal control. The primers used were as follows: Myosin Id forward,

98 ATTCGAACACCCCGTACACT-3'; Myosin Id reverse, 5'-TTGGTCCTCTTGTACCGCAT-3';

99 HPRT   forward,   5'-TTGTTGTTGGATATGCCCTTGACTA-3';   and   HPRT   reverse,

100 5'-AGGCAGATGGCCACAGGACTA-3'.

101

102 *Immunoblot analysis*

103 To obtain a synaptosomal fraction, adult mouse cerebra were homogenized in ice-cold TEVP

104 buffer (10 mM Tris, pH 7.5, 1 mM EDTA, 1 mM EGTA, 320 mM sucrose) containing a cOmplete

105 Protease Inhibitor Cocktail (Roche) and were centrifuged at 1000 × g for 10 minutes at 4 °C to

106 remove nuclei and large debris. The supernatant (S1) was centrifuged at 10,000 × g for 20 minutes at

107 4 °C. The resulting supernatant (S2) was collected as a cytoplasmic faction, and the remaining pellet

108 (P2), a crude synaptosomal fraction, was solubilized with 1% SDS in TEVP buffer. HEK293T cells

109 were lysed with RIPA buffer (50 mM Tris, pH 8.0, 150 mM NaCl, 1% Triton X-100, 0.1% SDS)

110 containing the protease inhibitors.

111 The lysates were mixed with Laemmli sample buffer (Bio-Rad) and heated for 3 minutes at 95°C.

112 The samples were electrophoresed by SDS-PAGE and transferred to PVDF membranes. The

113 membranes were blocked with 5% skim milk in TBS-0.05% Tween-20 for 30 minutes at room

114 temperature and incubated with primary antibodies overnight at 4 °C. The antibodies used were as

115 follows: anti-GFP (1:1000, A11122; Invitrogen), anti-myosin Id (1:200, sc-66982, Santa Cruz

116 Biotechnology), anti-PSD-95 (1:2000, ab13552; Abcam) and anti-β-actin (1:5000, A5441, Sigma).

117   The following day, HRP-linked secondary antibodies (1:10,000, Cell Signaling Technology) and

118   Immobilon HRP Chemiluminescence HRP substrate (Millipore) were used for detection. The bands

119   were visualized with a C-DiGit Blot Scanner (LI-COR Bioscience) and quantified with Image Studio

120   Digits software (LI-COR Bioscience). The signal intensity of each sample was normalized to that of

121   β-actin.

122

123   *Immunocytochemistry*

124   The cells on coverslips were fixed with 4% paraformaldehyde in PBS for 15 minutes at room

125   temperature. The cells were then permeabilized and blocked with 3% normal goat serum plus 0.1%

126   Triton X-100 in PBS for 1 hour at room temperature and incubated with primary antibodies

127   overnight at 4 °C. The antibodies used were as follows: anti-myosin Id (1:200, sc-66982, Santa Cruz

128   Biotechnology) and anti-PSD-95 (1:2000, ab13552; Abcam). The following day, the cells were

129   washed with PBS-0.05% Tween-20 and then incubated with Alexa Fluor 568-conjugated secondary

130   antibody (Molecular Probes) for 1 hour at room temperature. For F-actin staining, the cells were

131   incubated with Alexa Fluor 568-phalloidin (Molecular Probes) for 30 minutes at room temperature.

132   The coverslips were mounted onto glass slides using a mounting medium.

133

134 *Image analysis*

135　　Fluorescence images were acquired on a LSM510 laser confocal microscope (Carl Zeiss) with a

136　40×/1.2 NA water-immersion objective and analyzed with Image J software (NIH). Each area of

137　interest was enclosed manually and its fluorescence intensity was quantified. The areas of

138　pseudopodia were determined based on F-actin accumulation. The areas of cytoplasm were enclosed

139　except for pseudopodia and nuclei. The areas of dendritic spines were determined based on the

140　morphology visualized by mCherry (Hotulainen and Hoogenraad, 2010).

141

142 *Statistical analysis*

143　　All data are expressed as means ± SEMs. Differences between the two groups were analyzed using

144　a Student *t* test. For comparison within the same samples, a paired *t* test was applied. For multiple

145　comparisons, the Tukey Honest Significant Differences (HSD) test or the Dunnett test was applied.

146　All statistical analyses were performed using R software (http://www.r-project.org). Probability

147　values less than 0.05 were considered significant.

148

149　**Results**

150　*Myosin Id is enriched in the synaptosomal fraction of mouse brain.*

151   It has already been reported that myosin Id is expressed in neurons (Benesh et al., 2012). To test

152   whether there is a regional preference for its expression within the brain, we collected RNA from

153   different subregions of the mouse brain and analyzed myosin Id mRNA expression using qRT-PCR.

154   We found that myosin Id was expressed throughout the mouse brain, but it was more highly

155   expressed in the striatum, thalamus, and brain stem (Fig. 1A). Next, we examined myosin Id mRNA

156   expression in the whole brain at different ages. At P28, the young adult stage, it was expressed twice

157   as much as at P0 (Fig. 1B). Notably, oligodendrocytes also express myosin Id (Yamazaki et al., 2014).

158   The upregulation of myosin Id at P28 could be attributed to postnatal proliferation of

159   oligodendrocytes. Thus, we prepared primary hippocampal neurons to minimize the effect of

160   oligodendrocytes. As a result, myosin Id mRNA levels were unchanged between days *in vitro* (DIV)

161   1, 7, and 14 (Fig. 1C). Furthermore, to investigate the localization of myosin Id protein, we prepared

162   synaptosomal and cytoplasmic fractions from adult mouse cerebra. Immunoblot analysis with

163   anti-myosin Id antibody has revealed that myosin Id protein is significantly enriched in the

164   synaptosomal fraction compared to the cytoplasmic fraction (Fig. 1D, E) in a similar manner to

165   PSD-95, a well-known postsynaptic marker. These data suggest that myosin Id is a synapse-related

166   molecule.

167

168   *Myosin Id localizes in the F-actin-rich pseudopodia of HEK293T cells.*

169   To characterize the subcellular localization of myosin Id protein, we prepared an expression vector

170   that produces EGFP-tagged myosin Id protein. We transfected HEK293T cells with this vector and

171   confirmed successful expression of EGFP-myosin Id protein as shown by immunoblot analysis (Fig.

172   2A). In addition, immunocytochemical analyses showed that the GFP signals were highly enriched in

173   the F-actin-rich pseudopodia (Fig. 2B).

174

175   *Myosin Id localizes in the dendritic spines of primary hippocampal neurons.*

176   Given that dendritic spines are rich in the actin cytoskeleton (Cingolani and Goda, 2008), we

177   tested whether myosin Id accumulates there. We transfected primary hippocampal neurons at DIV13,

178   when the dendritic spines are formed, with an EGFP-myosin Id vector. An mCherry-C1 vector was

179   co-transfected as a reference. At 24 hours after transfection, we examined the fluorescence intensities

180   of both EGFP and mCherry at the same spine. The spine/shaft ratio of GFP was statistically higher

181   than that of mCherry at the same spine (Fig. 3A, B), which demonstrated that myosin Id is enriched

182   in dendritic spines. Consistent with this, GFP fluorescence in the PSD-95-positive puncta (dendritic

183   spines) was significantly higher than that in the neighboring PSD-95-negative shafts (Fig. 3C, D).

184   These results reveal that myosin Id protein localizes in dendritic spines.

185

Deletion of the TH1 domain drastically diminishes its colocalization with F-actin in the

pseudopodia.

To identify a region responsible for its localization, we created mutant vectors lacking specific

regions (Fig. 4A). To search for a possible actin-binding site, we identified the conserved sequence

(residues 584–594) corresponding to the actin-binding site of *Drosophila* homolog myosin IA

(Morgan et al., 1994). Deletion of residues 584–594 (Δ584–594) reduced its accumulation in the

F-actin-rich pseudopodia, yet the reduction was marginal (Fig. 4B, C). Surprisingly, deletion of the

TH1 domain (ΔTH1) drastically diminished its accumulation in the pseudopodia. A C-terminal

fragment consisting of the IQ motifs and the TH1 domain (IQ + TH1) localized mainly in the nuclei.

This nuclear localization is similar to the findings of a previous study with myosin Ig (Patino-Lopez

et al., 2010), which has higher homology to myosin Id (59%, ClastalW;

http://www.genome.jp/tools-bin/clustalw) than do any other class I myosins (29−37%). Deletion of

the N-terminal portion might unmask a cryptic nuclear localization signal. Notably, the IQ + TH1

fragment was also enriched in the pseudopodia.

200

"Signature basic residues" in the TH1 domain are critical for its colocalization with F-actin.

202   The TH1 domain in class I myosins commonly includes the pleckstrin homology (PH) domain,

203   which is capable of binding to phospholipids (McConnell and Tyska, 2010). A previous study with

204   myosin Ic determined the conserved basic residues ("signature basic residues") that are critical for its

205   binding capacity (Hokanson et al., 2006). We created two additional mutant vectors of myosin Id in

206   which each of the corresponding basic residues is substituted with alanine (K865A or R875A).

207   Notably, both of the mutant forms displayed diminished colocalization with F-actin in the

208   pseudopodia (Fig 5A, B). These results reveal that the TH1 domain is critical for its colocalization

209   with F-actin.

210

211   *The TH1 domain is critical for distribution of myosin Id from the soma to the dendrites and for its*

212   *enrichment in dendritic spines.*

213   To test whether the TH1 domain is important for localization of myosin Id even in neurons, we

214   transfected primary hippocampal neurons at DIV13 with full-length or ΔTH1 vectors. Notably, the

215   ΔTH1 fragment was less distributed from the soma to the dendrites than was full-length myosin Id

216   (Fig. 6A, B). In addition, the ΔTH1 fragment showed diminished accumulation in dendritic spines as

217   evidenced by reduction in the GFP fluorescence ratio of the spines to the shafts (Fig. 6C, D). These

218   results suggest that the TH1 domain is critical for the distribution of myosin Id from the soma to the

219   dendrites and for its enrichment in dendritic spines.

220

221   **Discussion**

222   In this study, we have revealed that myosin Id localizes in the dendritic spines of neurons. Domain

223   analysis suggested that the TH1 domain is critical for distribution of myosin Id in dendritic spines.

224   To our knowledge, ours is the first study to describe the subcellular localization of myosin Id in

225   neurons.

226   Fine-tuning of synaptic transmission in accordance with environmental stimuli, namely synaptic

227   plasticity, underlies brain functions such as learning and memory. A number of molecules in dendritic

228   spines are involved in regulation of synaptic plasticity (Caroni et al., 2012; Koleske, 2013).

229   Abnormalities in synaptic transmission have been proposed to underlie the pathogenesis of ASD

230   (Barak and Feng, 2016). Clinical studies have shown that individuals with ASD exhibit a higher

231   density of dendritic spines than do age-matched controls (Penzes et al., 2011). In addition,

232   *Fmr1*-knockout mice, a model for fragile X syndrome, exhibit enhanced mGluR5-dependent

233   long-term depression accompanied by a higher density of dendritic spines in the hippocampi (Dölen

234   et al., 2007; Huber et al., 2002). These studies highlighted the importance of understanding the

235   regulatory mechanisms underlying the dynamics of dendritic spines. Combined with the linkage

236   analysis suggesting myosin Id as a potential risk gene for ASD (Stone et al., 2007), our results

237   showing that myosin Id is enriched in dendritic spines raise the possibility that myosin Id regulates

238   synaptic transmission in dendritic spines and, furthermore, that its dysfunction would result in ASD.

239   Further analyses such as by means of electrophysiological and behavioral experiments will be

240   required to test this possibility.

241   In this study, both deletion and substitution of the TH1 domain drastically diminished its

242   enrichment in the F-actin-rich pseudopodia. Although the TH1 domain includes the PH domain,

243   which is capable of binding to anionic phospholipids (Hokanson et al., 2006), it is unlikely that its

244   binding to phospholipids solely determines the localization of myosin Id because the GFP signals did

245   not accumulate on the plasma membrane. Unexpectedly, deletion of the conserved domain

246   corresponding to the actin-binding site in *Drosophila* homolog myosin IA (Morgan et al., 1994)

247   resulted in marginal reduction of the enrichment in pseudopodia. These results indicate that this

248   conserved domain is not critical for its actin binding and, furthermore, that actin-binding sites in the

249   motor domain of mammalian myosin Id remain unclear. Interestingly, our study suggests that the

250   TH1 domain critically mediates binding of mammalian myosin Id to F-actin. Previous studies

251   showing that the PH domain interacts with F-actin (Macia et al., 2008; Yao et al., 1999) support our

252   results. Further biophysical and biochemical studies will be required to clarify how myosin Id

253 interacts with actin filaments.

254 Neurons have a specialized transport system to deliver dendritic molecules efficiently throughout

255 the multiple and highly branched dendrites. For this delivery, neurons use motor proteins, that is,

256 kinesins, dyneins, and myosins. These motor proteins carry their cargo to the destination by moving

257 along cytoskeletons (microtubules or actin filaments) (Hirokawa et al., 2010). Actin filaments exist

258 not only in the dendritic spines but also in the dendritic shafts as long bundles (Konietzny et al.,

259 2017). Previous studies have shown that an actin-depolymerizing factor, cytochalasin D, disturbs the

260 dendritic localization of some specific molecules (Balasanyan and Arnold, 2014; Lewis et al., 2009),

261 which suggests that actin filaments offer some paths for dendritic transport. In those previous studies,

262 myosin Va was suggested as a carrier in this actin-based dendritic transport. In our study, the ΔTH1

263 were less distributed from the soma to the dendrites than was the full-length form. Combined with

264 the fact that ΔTH1 is defective in binding to F-actin, it could be assumed that myosin Id moves to the

265 dendrites along actin filaments through the TH1 domain by its own energy. However, it cannot be

266 ruled out that myosin Id is transported to dendrites by different molecules. Additional analysis of a

267 mutant form with defective ATPase activity that cannot use the energy of ATP would provide us with

268 useful information.

269 At present, the function of myosin Id in neurons remains to be uncovered. In a variety of cell types,

270 class I myosins work as a linker between actin filaments and phospholipids (McIntosh and Ostap,

271 2016). In fact, class I myosins prefer to localize actin-rich protrusions such as the microvilli of

272 enterocytes (myosins Ia and Id) (Tyska et al., 2005; Tyska and Mooseker, 2004), stereocilia of

273 auditory hair cells (myosin Ic) (Holt et al., 2002), and foot processes of podocytes (myosin Ie) (Mele

274 et al., 2011), where they are involved in maintenance of membrane tension. In addition, class I

275 myosins have been proposed to dock or tether vesicles to the plasma membrane (Boguslavsky et al.,

276 2012). If myosin Id shares these functions, it could be possible that myosin Id modulates synaptic

277 transmission by regulating dendritic spine architecture or vesicular transport.

278   In conclusion, myosin Id, a member of the class I myosins, localizes in dendritic spines through

279 the TH1 domain. Our study also provides the possibility that the TH1 domain, rather than the motor

280 domain, includes a critical actin-binding site in myosin Id.

281

282 **Author contributions**

283   R.K. and Y.T. designed the experiments. R.K. and S.T. performed the experiments. R.K. analyzed

284 the data and wrote the manuscript.

285

286 **Conflicts of interest**

287   The authors declare no competing financial interests.

288

296

297

298   **References**

299   Balasanyan, V., Arnold, D.B., 2014. Actin and myosin-dependent localization of mRNA to dendrites.

300   PLoS One 9. https://doi.org/10.1371/journal.pone.0092349

301   Barak, B., Feng, G., 2016. Neurobiology of social behavior abnormalities in autism and Williams

302   syndrome. Nat. Neurosci. 19, 647–655. https://doi.org/10.1038/nn.4276

303   Benesh, A.E., Fleming, J.T., Chiang, C., Carter, B.D., Tyska, M.J., 2012. Expression and localization

304 of myosin-1d in the developing nervous system. Brain Res. 1440, 9–22.

305 https://doi.org/10.1016/j.brainres.2011.12.054

306 Benesh, A.E., Nambiar, R., McConnell, R.E., Mao, S., Tabb, D.L., Tyska, M.J., 2010. Differential

307 Localization and Dynamics of Class I Myosins in the Enterocyte Microvillus. Mol. Biol. Cell 21,

308 970–978. https://doi.org/10.1091/mbc.E09-07-0638

309 Boguslavsky, S., Chiu, T., Foley, K.P., Osorio-Fuentealba, C., Antonescu, C.N., Bayer, K.U., Bilan,

310 P.J., Klip, A., 2012. Myo1c binding to submembrane actin mediates insulin-induced tethering of

311 GLUT4 vesicles. Mol. Biol. Cell 23, 4065–4078. https://doi.org/10.1091/mbc.E12-04-0263

312 Bose, A., Robida, S., Furcinitti, P.S., Chawla, A., Fogarty, K., Corvera, S., Czech, M.P., 2004.

313 Unconventional myosin Myo1c promotes membrane fusion in a regulated exocytic pathway.

314 Mol. Cell. Biol. 24, 5447–5458. https://doi.org/10.1128/MCB.24.12.5447-5458.2004

315 Caroni, P., Donato, F., Muller, D., 2012. Structural plasticity upon learning: Regulation and

316 functions. Nat. Rev. Neurosci. 13, 478–490. https://doi.org/10.1038/nrn3258

317 Cingolani, L.A., Goda, Y., 2008. Actin in action: The interplay between the actin cytoskeleton and

318 synaptic efficacy. Nat. Rev. Neurosci. 9, 344–356. https://doi.org/10.1038/nrn2373

319 Dölen, G., Osterweil, E., Rao, B.S.S., Smith, G.B., Auerbach, B.D., Chattarji, S., Bear, M.F., 2007.

320 Correction of Fragile X Syndrome in Mice. Neuron 56, 955–962.

321   https://doi.org/10.1016/j.neuron.2007.12.001

322 Gu, J., Lee, C.W., Fan, Y., Komlos, D., Tang, X., Sun, C., Yu, K., Hartzell, H.C., Chen, G.,

323   Bamburg, J.R., Zheng, J.Q., 2010. ADF/cofilin-mediated actin dynamics regulate AMPA

324   receptor trafficking during synaptic plasticity. Nat. Neurosci. 13, 1208–1215.

325   https://doi.org/10.1038/nn.2634

326 Hirokawa, N., Niwa, S., Tanaka, Y., 2010. Molecular motors in neurons: Transport mechanisms and

327   roles in brain function, development, and disease. Neuron 68, 610–638.

328   https://doi.org/10.1016/j.neuron.2010.09.039

329 Hokanson, D.E., Laakso, J.M., Lin, T., Sept, D., Ostap, E.M., 2006. Myo1c Binds Phosphoinositides

330   through a Putative Pleckstrin Homology Domain. Mol. Biol. Cell 17, 4856–4865.

331   https://doi.org/10.1091/mbc.E06-05-0449

332 Hokanson, D.E., Ostap, E.M., 2006. Myo1c binds tightly and specifically to phosphatidylinositol

333   4,5-bisphosphate and inositol 1,4,5-trisphosphate. Proc. Natl. Acad. Sci. U. S. A. 103, 3118–

334   3123. https://doi.org/10.1073/pnas.0505685103

335 Holt, J.R., Gillespie, S.K.H., Provance, D.W., Shah, K., Shokat, K.M., Corey, D.P., Mercer, J.A.,

336   Gillespie, P.G., 2002. A chemical-genetic strategy implicates myosin-1c in adaptation by hair

337   cells. Cell 108, 371–381. https://doi.org/10.1016/S0092-8674(02)00629-3

338   Hotulainen, P., Hoogenraad, C.C., 2010. Actin in dendritic spines: Connecting dynamics to function.

339   J. Cell Biol. 189, 619–629. https://doi.org/10.1083/jcb.201003008

340   Hozumi, S., Maeda, R., Taniguchi, K., Kanai, M., Shirakabe, S., Sasamura, T., Spéder, P., Noselli, S.,

341   Aigaki, T., Murakami, R., Matsuno, K., 2006. An unconventional myosin in Drosophila

342   reverses the default handedness in visceral organs. Nature 440, 798–802.

343   https://doi.org/10.1038/nature04625

344   Huber, K.M., Gallagher, S.M., Warren, S.T., Bear, M.F., 2002. Altered synaptic plasticity in a mouse

345   model of fragile X mental retardation. Proc. Natl. Acad. Sci. 99, 7746–7750.

346   https://doi.org/10.1073/pnas.122205699

347   Kneussel, M., Wagner, W., 2013. Myosin motors at neuronal synapses: Drivers of membrane

348   transport and actin dynamics. Nat. Rev. Neurosci. 14, 233–247. https://doi.org/10.1038/nrn3445

349   Koleske, A.J., 2013. Molecular mechanisms of dendrite stability. Nat. Rev. Neurosci. 14, 536–550.

350   https://doi.org/10.1038/nrn3486

351   Komaba, S., Coluccio, L.M., 2010. Localization of myosin 1b to actin protrusions requires

352   phosphoinositide binding. J. Biol. Chem. 285, 27686–27693.

353   https://doi.org/10.1074/jbc.M109.087270

354   Konietzny, A., Bär, J., Mikhaylova, M., 2017. Dendritic Actin Cytoskeleton: Structure, Functions,

355   and Regulations. Front. Cell. Neurosci. 11, 1–10. https://doi.org/10.3389/fncel.2017.00147

356   Lewis, T.L., Mao, T., Svoboda, K., Arnold, D.B., 2009. Myosin-dependent targeting of

357   transmembrane proteins to neuronal dendrites. Nat. Neurosci. 12, 568–576.

358   https://doi.org/10.1038/nn.2318

359   Macia, E., Partisani, M., Favard, C., Mortier, E., Zimmermann, P., Carlier, M.F., Gounon, P., Luton,

360   F., Franco, M., 2008. The pleckstrin homology domain of the Arf6-specific exchange factor

361   EFA6 localizes to the plasma membrane by interacting with phosphatidylinositol

362   4,5-bisphosphate and F-actin. J. Biol. Chem. 283, 19836–19844.

363   https://doi.org/10.1074/jbc.M800781200

364   McConnell, R.E., Tyska, M.J., 2010. Leveraging the membrane - cytoskeleton interface with

365   myosin-1. Trends Cell Biol. 20, 418–426. https://doi.org/10.1016/j.tcb.2010.04.004

366   McIntosh, B.B., Ostap, E.M., 2016. Myosin-I molecular motors at a glance. J. Cell Sci. 129, 2689–

367   2695. https://doi.org/10.1242/jcs.186403

368   Mele, C., Iatropoulos, P., Donadelli, R., Calabria, A., Maranta, R., Cassis, P., Buelli, S., Tomasoni,

369   S., Piras, R., Krendel, M., Bettoni, S., Morigi, M., Delledonne, M., Pecoraro, C., Abbate, I.,

370   Capobianchi, M.R., Hildebrandt, F., Otto, E., Schaefer, F., Macciardi, F., Ozaltin, F., Emre, S.,

371   Ibsirlioglu, T., Benigni, A., Remuzzi, G., Noris, M., 2011. MYO1E Mutations and Childhood

372   Familial Focal Segmental Glomerulosclerosis. N. Engl. J. Med. 365, 295–306.

373   https://doi.org/10.1056/NEJMoa1101273

374   Morgan, N.S., Skovronsky, D.M., Artavanis-Tsakonas, S., Mooseker, M.S., 1994. The Molecular

375   Cloning and Characterization of Drosophila melanogaster Myosin-IA and Myosin-IB. J. Mol.

376   Biol. 239, 347–356. https://doi.org/10.1006/jmbi.1994.1376

377   Patino-Lopez, G., Aravind, L., Dong, X., Kruhlak, M.J., Ostap, E.M., Shaw, S., 2010. Myosin 1G is

378   an abundant class I myosin in lymphocytes whose localization at the plasma membrane depends

379   on its ancient divergent pleckstrin homology (PH) domain (Myo1PH). J. Biol. Chem. 285,

380   8675–8686. https://doi.org/10.1074/jbc.M109.086959

381   Penzes, P., Cahill, M.E., Jones, K.A., Vanleeuwen, J.E., Woolfrey, K.M., 2011. Dendritic spine

382   pathology in neuropsychiatric disorders. Nat. Neurosci. 14, 285–293.

383   https://doi.org/10.1038/nn.2741

384   Rex, C.S., Gavin, C.F., Rubio, M.D., Kramar, E.A., Chen, L.Y., Jia, Y., Huganir, R.L., Muzyczka,

385   N., Gall, C.M., Miller, C.A., Lynch, G., Rumbaugh, G., 2010. Myosin IIb Regulates actin

386   dynamics during synaptic plasticity and memory formation. Neuron 67, 603–617.

387   https://doi.org/10.1016/j.neuron.2010.07.016

388   Ryu, J., Liu, L., Wong, T.P., Wu, D.C., Burette, A., Weinberg, R., Wang, Y.T., Sheng, M., 2006. A

389   critical role for myosin IIB in dendritic spine morphology and synaptic function. Neuron 49,

390   175–182. https://doi.org/10.1016/j.neuron.2005.12.017

391 Spence, E.F., Kanak, D.J., Carlson, B.R., Soderling, S.H., 2016. The Arp2/3 Complex Is Essential

392   for Distinct Stages of Spine Synapse Maturation, Including Synapse Unsilencing. J. Neurosci.

393   36, 9696–9709. https://doi.org/10.1523/JNEUROSCI.0876-16.2016

394 Stone, J.L., Merriman, B., Cantor, R.M., Geschwind, D.H., Nelson, S.F., 2007. High density SNP

395   association study of a major autism linkage region on chromosome 17. Hum. Mol. Genet. 16,

396   704–715. https://doi.org/10.1093/hmg/ddm015

397 Tyska, M.J., Mackey, A.T., Huang, J.-D., Copeland, N.G., Jenkins, N.A., Mooseker,   and M.S.,

398   2005. Myosin-1a Is Critical for Normal Brush Border Structure and Composition. Mol. Biol.

399   Cell 16, 2443–2457. https://doi.org/10.1091/mbc.E04-12-1116

400 Tyska, M.J., Mooseker, M.S., 2004. A role for myosin-1A in the localization of a brush border

401   disaccharidase. J. Cell Biol. 165, 395–405. https://doi.org/10.1083/jcb.200310031

402 Tyska, M.J., Mooseker, M.S., 2002. MYO1A (brush border myosin I) dynamics in the brush border

403   of LLC-PK1-CL4 cells. Biophys. J. 82, 1869–1883.

404   https://doi.org/10.1016/S0006-3495(02)75537-9

405 Yamazaki, R., Ishibashi, T., Baba, H., Yamaguchi, Y., 2014. Unconventional myosin ID is expressed

406 in myelinating oligodendrocytes. J. Neurosci. Res. 92, 1286–1294.

407 https://doi.org/10.1002/jnr.23419

408 Yao, L., Janmey, P., Frigeri, L.G., Han, W., Fujita, J., Kawakami, Y., Apgar, J.R., Kawakami, T.,

409 1999. Pleckstrin homology domains interact with filamentous actin. J. Biol. Chem. 274, 19752–

410 19761. https://doi.org/10.1074/jbc.274.28.19752

411

Figure legends

Fig. 1. Myosin Id is enriched in the synaptosomal fraction of mouse brain. (A) qRT-PCR analysis for

myosin Id mRNA in the subregions of mouse brain at 8 weeks of age. n = 4 per group. Data are

expressed relative to the mean value of all samples. (B) Myosin Id mRNA expression in the whole

brain during postnatal development. n = 4 per each group. Data are expressed relative to the P0. *$p <$

0.05, Dunnett multiple comparison test (vs P0). (C) Myosin Id mRNA expression in primary

hippocampal neurons at different days *in vitro* (DIV). Data are expressed relative to the DIV 1. n = 3

per group. (D) Immunoblot analysis of cytoplasmic and synaptosomal fractions prepared from adult

mouse cerebra. Myosin Id protein is significantly enriched in the synaptosomal fraction. PSD-95 is a

postsynaptic marker. (E) Signal intensity of the immunoblot analysis. Data are expressed as a ratio to

β-actin. n = 3 cerebra. *$p < 0.05$, paired *t* test.

Fig. 2. Myosin Id localizes in the F-actin-rich pseudopodia of HEK293T cells. (A) Immunoblot

analysis for EGFP-myosin Id expression by HEK293T. Anti-GFP antibody was used as the primary

antibody. A band of EGFP-myosin Id protein appears at approximately 150 kDa (arrow). (B)

Confocal images of HEK293T cells at 24 hours after transfection. EGFP-myosin Id (green) was

overlapped with F-actin (red) in the pseudopodia (arrowheads). Scale bar: 20 μm.

429

Fig. 3. Myosin Id localizes in the dendritic spines of primary hippocampal neurons. (A) Confocal

images of primary hippocampal neurons at DIV14 transfected with both EGFP-myosin Id (green)

and mCherry (red), which was used as a reference. The lower panels show higher magnification

images of the square areas in the upper panels. The yellow and white circles indicate the areas of the

spines and the neighboring shafts, respectively. Scale bars: upper panels, 50 μm; lower panels, 5 μm.

(B) A scatterplot representing the fluorescence ratio of the spines to the shafts. GFP fluorescence

(y-axis) is biased to the spine as evidenced by its significantly higher fluorescence ratio than that of

mCherry (x-axis) at the same spines. n = 79 spines (6 neurons). $p < 0.05$, paired t test. (C)

EGFP-myosin Id (green) colocalizes with PSD-95 (red), a postsynaptic marker. Scale bar: 5 μm. (D)

GFP fluorescence in the PSD-95-positive puncta (spines) is significantly higher than that in the

neighboring PSD-95-negative shafts. n = 77 puncta (4 neurons). *$p < 0.05$, paired t test.

441

Fig. 4. Deletion of the TH1 domain drastically diminishes its colocalization with F-actin in the

pseudopodia. (A) Schematic protein structures of full-length and mutant forms of myosin Id. The

conserved region (residues 584−594) corresponding to the actin-binding site of *Drosophila* homolog

myosin IA (Δ584−594), the TH1 domain (ΔTH1), or the motor domain (IQ + TH1) was deleted in

446 each mutant vector. (B) Confocal images of HEK293T cells transfected with full-length or mutant

447 forms of myosin Id. Scale bar: 20 μm. Arrowheads indicate the F-actin-rich pseudopodia (red). (C)

448 GFP fluorescence ratio of pseudopodia to cytoplasm. n = 10–12 cells per group. *$p < 0.05$, **$p <$

449 0.01, ***$p < 0.001$, Tukey HSD test.

450

451 Fig. 5. "Signature basic residues" in the TH1 domain are critical for its colocalization with F-actin.

452 (A) Confocal images of HEK293T cells transfected with full-length or mutant forms in which each

453 of the "signature basic residues" was substituted with alanine (K865A, R875A). Scale bar: 20 μm.

454 (B) GFP fluorescence ratio of pseudopodia to cytoplasm. n = 10 cells per group. * $p < 0.05$, Tukey

455 HSD test.

456

457 Fig. 6. The TH1 domain is critical for distribution of myosin Id from the soma to the dendrites and

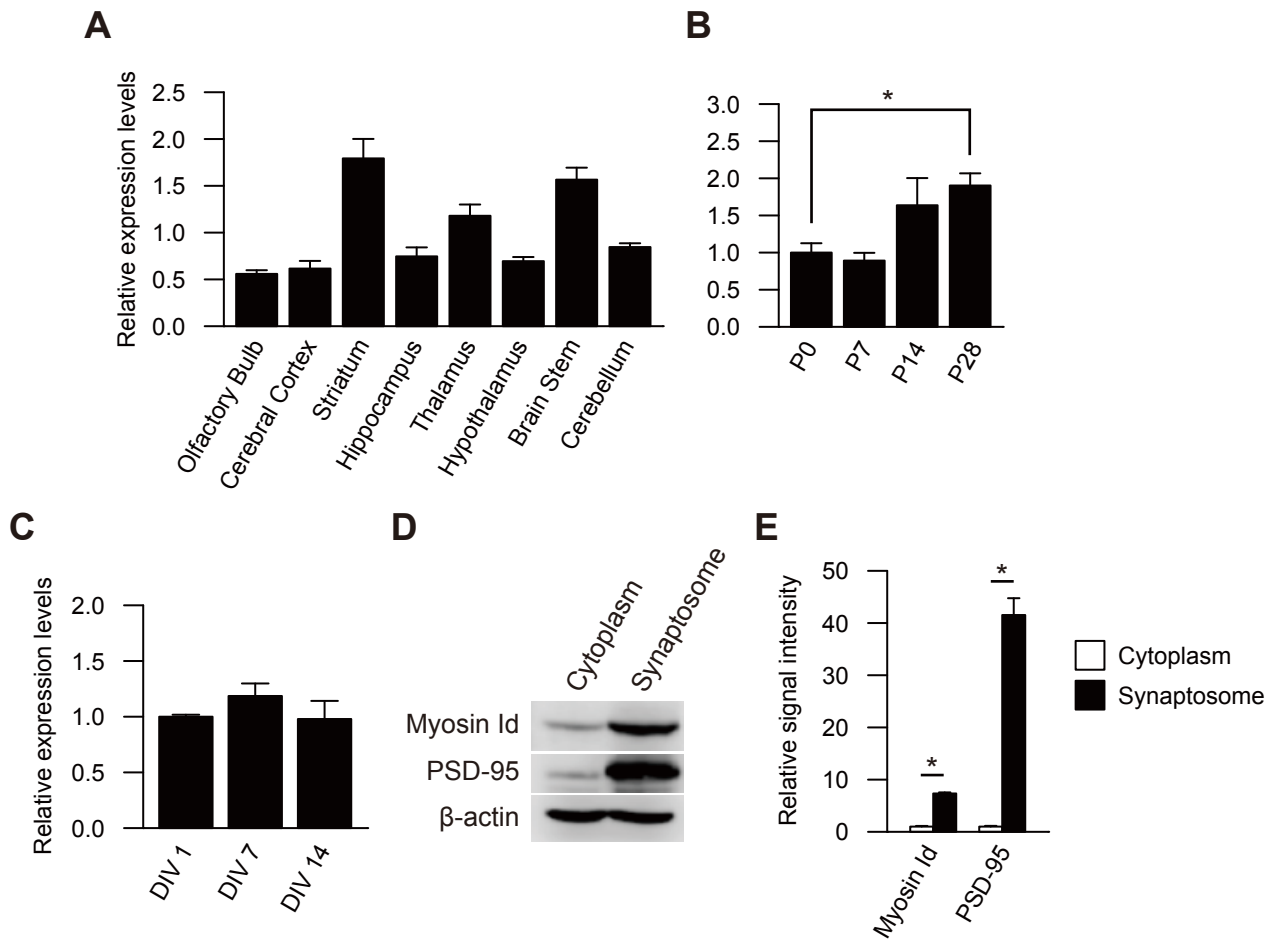458 for its enrichment in the dendritic spines of primary hippocampal neurons. (A) Primary hippocampal

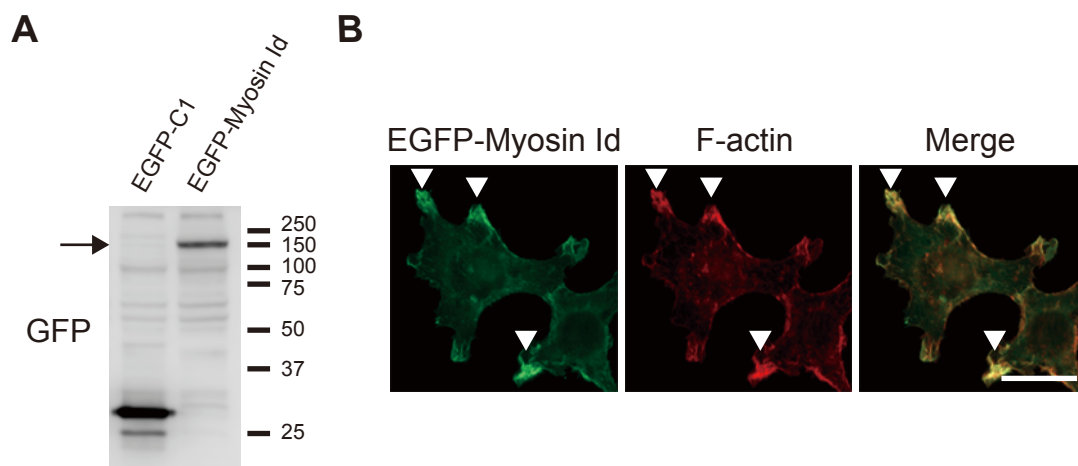459 neurons at DIV14 transfected with full-length myosin Id or ΔTH1 vectors. Scale bar: 50 μm. (B)

460 GFP fluorescence ratio of dendrites to nuclei. n = 6 neurons per group. *$p < 0.05$, Student t test. (C)

461 Confocal images of dendritic spines. Scale bar: 5 μm. (D) GFP fluorescence ratio of spines to shafts.

462 mCherry fluorescence was used as a reference. n = 90 (full-length) or 91 (ΔTH1) spines from 4

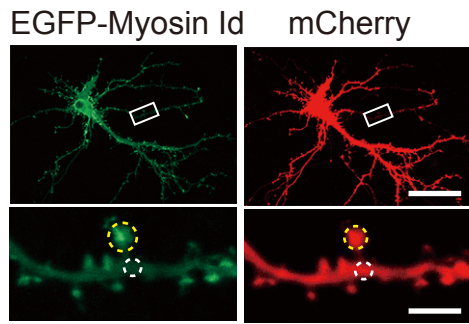463 neurons per group. *$p < 0.05$, Student t test.

Koshida et al., Fig 2.
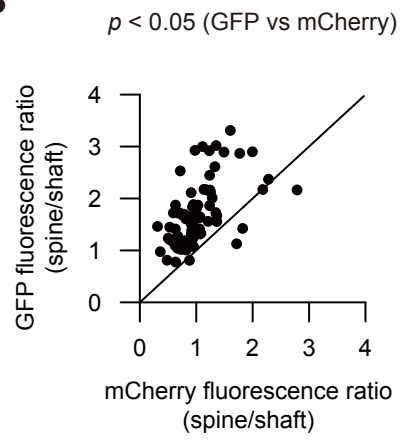
A

EGFP-C1
EGFP-Myosin Id

250
150
100
75

GFP

50

37

25

B

EGFP-Myosin Id	F-actin	Merge

Koshida et al., Fig 3.

A

EGFP-Myosin Id   mCherry

B

p < 0.05 (GFP vs mCherry)

GFP fluorescence ratio (spine/shaft)

mCherry fluorescence ratio (spine/shaft)

C

EGFP-Myosin Id   PSD-95   Merge

D

Relative GFP fluorescence

*

PSD-95⁻ shaft   PSD-95⁺ spine

A

Full-length 1 Motor Domain IQ TH1 1006

Δ584−594 ×

ΔTH1 720

IQ + TH1 570

B

EGFP-Myosin Id | F-actin | Merge

Full-length

Δ584-594

ΔTH1

IQ + TH1

C

GFP fluorescence ratio (pseudopodia/cytoplasm)

A

B

A

EGFP-Myosin Id   mCherry

Full-length

ΔTH1

B

C

EGFP-Myosin Id   mCherry

Full-length

ΔTH1

D